Langmuir

Article

pubs.acs.org/Langmuir

Enhancing CaP Biomimetic Growth on TiO_2 Cuboids Nanoparticles via Highly Reactive Facets

Juan M. Ruso,[†] Valeria Verdinelli,[‡] Natalia Hassan,[§] Olga Pieroni,[‡] and Paula V. Messina*[,‡]

[†]Soft Matter and Molecular Biophysics Group, Department of Applied Physics, University of Santiago de Compostela, Santiago de Compostela, 15782, Spain

[‡]Department of Chemistry, Universidad Nacional del Sur, (8000) Bahía Blanca, Argentina, INQUISUR-CONICET

[§]Laboratoire Physico-chimie des Electrolytes, Colloides et Sciences Analytiques (PECSA), Université Pierre et Marie Curie, 75252 Paris, France

Supporting Information

ABSTRACT: Pure decahedral anatase TiO_2 particles with high content of reactive {001} facets were obtained from titanium(IV) tetrachloride ($TiCl_4$) using a microemulsions droplet system at specific conditions as chemical microreactor. The product was systematically characterized by X-ray diffraction, field-emission scanning and transmission electron microscopy (FE-SEM, TEM), N_2 adsorption−desorption isotherms, FT-IR and UV−vis spectroscopy, and photoluminescence studies. The obtained cuboids around 90 nm in size have a uniform and dense surface morphology with a BET specific surface area of 11.91 $m^2\ g^{-1}$ and a band gap energy (3.18 eV) slightly inferior to the anatase dominated by the less-reactive {101} surface (3.20 eV). The presence of reactive facets on titania anatase favors the biomimetic growth of amorphous tricalcium phosphate after the first day of immersion in simulated human plasma. The results presented here can facilitate and improve the integration of anchored implants and enhance the biological responses to the soft tissues.

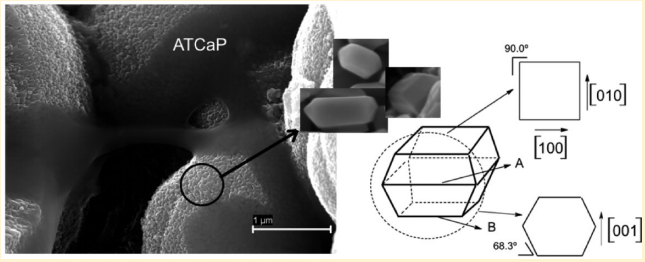

INTRODUCTION

Anatase titanium dioxide (TiO_2) is one of the most important semiconductors, playing a central role in many industrial applications such as photosplitting of water,[1] photocatalysis,[2] photovoltaic devices,[3] sensors,[4] mesoporous membranes,[5] gate oxides in metal-oxide-semiconductor field effect transistors,[6] granting,[7] and antifogging and self-cleaning coatings.[8] Most of these applications require not only the control of the size and shape of the nanostructures but also the control of the facets exposed on the surface. For anatase TiO_2, both theoretical and experimental studies found that minority {001} facets in the equilibrium state are especially reactive.[9] Unfortunately, most synthetic anatase crystals as well as those naturally occurring are dominated by the less-reactive (101) surface.[9] Recently, large high quality anatase crystals with a high percentage of {001} facets have been synthesized from TiF_4, using fluorine atom as capping agent in severe acidic conditions and a hydrothermal treatment at 180−200 °C.[10−12] Analogous TiO_2 anatase cuboids structures with smaller size were obtained by thermal oxidation of $TiCl_4$ at 1300 °C.[13]

Nowadays, titanium has found applications in biology and medicine: cytotoxicity toward some tumors under ultraviolet light excitation[14,15] or as bone repairing material in orthopedics and dentistry.[16] The use of titanium as biomaterial is possible because of its very favorable biocompatibility with living tissues, excellent resistance to corrosion, and superior mechanical properties.[17] However, some of the potential biotechnological applications of Ti have a drawback: the lack of bioactivity, as it does not support cell adhesion and growth.[18]

As regards the interaction of bioactive materials with living bone, an apatite layer is required to be present on the surface of the material to act as a bonding interface and to enhance the bioactivity. Titanium containing calcium phosphate (CaP) coatings are designed to combine the favorable mechanical properties of titanium and the biological properties of calcium phosphate ceramics.[19−22]

In terms of the coatings microstructure, nanostructure is considered to be one of the most effective to provide excellent properties. There are several techniques to produce apatite coatings, such as plasma spraying,[23] the sol−gel method,[24] and the biomimetic method.[25] The biomimetic process to produce bone-like apatite coating is low temperature technique which imitates or "mimics" the natural biomineralization during bone formation in human and animals. Biocompatible apatite coatings are deposited to the substrates by immersion in simulated body fluid (SBF).[25] TiO_2 coatings on Ti and Ti alloys have been also shown to enhance the corrosion resistance and biocompatibility. TiO_2 has a tendency to absorb water at the surface, resulting in formation of titanium hydroxide groups. The basic Ti−OH groups were reported to induce

Received: October 10, 2012
Revised: January 25, 2013
Published: January 29, 2013

apatite nucleation and crystallization in SBF.[22] The apatite, however, is not biomimetically formed on a single crystal of TiO_2 rhombohedral anatase as reported by Li et al.[22,27]

In the present study, we report the use of a reverse microemulsion system to control the morphology of TiO_2 crystals during hydrothermal synthesis at 100 °C. We conducted phase behavior measurements on several systems to identify the proper synthesis conditions. The mixture was treated as a pseudoternary system with oil, aqueous, and surfactant components. n-Heptane was chosen as the oil phase. The aqueous phase was a TiO_2 synthesis mixture of water, $TiCl_4$, and sodium bis(2-ethylhexyl) sulfosuccinate in a molar ratio of 30:1.7:1. By the application of this simple microemulsion-based synthesis, pure anatase truncated bipyramid nanocrystallites around 90 nm in size with high proportion of reactive {001} facets, similar to those previously reported,[10−13] were obtained. In the second part of our work, we evaluated the proficiency of the synthesized reactive cuboids to favor CaP biomimetic growth in a simulated physiological media. Unlike most CaP coatings prepared at low temperature and by using supersaturated calcium phosphate solutions[28] that lead to hydroxyapatite (HA) layers, here we demonstrate that reactive facets on titania anatase favor the biomimetic growth of amorphous tricalcium phosphate (ATCaP) after the first day of immersion in simulated human plasma solutions. ATCaP is biologically present in soft-tissue calcifications,[29] and the experiments were performed thinking to the future use of the tested materials in improved three-dimensional scaffolds that merge the reactivity of anatase TiO_2 {001} facets and the osseointegration of ATCaP.

MATERIALS AND METHODS

Materials. Sodium bis(2-ethylhexyl) sulfosuccinate (Aerosol-OT, AOT, 99% Sigma), n-heptane (Merck, δ = 0.684 g cm^{-3}), and $TiCl_4$ (Carlo Erba, 99%, δ = 1.722 g cm^{-3}) were used without further purification. For microemulsion preparation, only triple-distilled water was used.

Methods. *Microemulsion System.* Experiments were performed on water/AOT/n-heptane microemulsion systems. Microemulsion systems of S_0 = 60 and W_0 = 30 were prepared, where W_0 is the ratio of water to surfactant molar concentrations and S_0 is the ratio of oil to surfactant molar concentration. As the critical micellization concentration (CMC) of AOT[30] in both oil and water is low compared with the concentration used here, it can be assumed that all the surfactant molecules are localized at the interface between water and oil. The microemulsions were prepared by mixing the appropriate amounts of water and AOT in a flask and left during 3 h to produce the surfactant hydration. Then, oil (n-heptane) was added, and the system was sonicated to produce the microemulsion. The resulting microemulsions were placed in Teflon-stoppered test tubes and left to equilibrate for 24 h at 40 °C before being used. We worked inside the L2 phase boundary, where the structures of the aggregates are spheres.[31]

Microemulsion-Mediated Hydrothermal Synthesis of TiO_2 Samples. To obtain the TiO_2 material, the direct injection of the titania precursor to the microemulsion followed by a hydrothermal treatment was performed: 1.4 mL of $TiCl_4$ (Ti^{4+}/AOT = 1.7; water/Ti^{4+} and oil/Ti^{4+} = 35) was added to the above described microemulsion and left three days at room temperature under stirring at 600 rpm to follow the reaction

$$TiCl_4 + 2H_2O \leftrightarrows TiO_2 + 4HCl$$

HCl and the excess of nonpolar solvent were eliminated by evaporation under vacuum. Then, the resulting gel was left for 24 h in an autoclave at 100 °C. The obtained materials were filtered and washed with triple-distilled water and left to dry at room temperature. Finally, it was calcined for 7 h at 640 °C in an air flux.

Characterization. *Field Emission Scanning Electron Microscopy (FE-SEM).* Field emission scanning electron microscopy (FE-SEM) was performed using a ZEISS FE-SEM ULTRA PLUS. To acquire all the SEM images a secondary electron detector (In lens) was used. The accelerating voltage (EHT) applied was 3.00 kV with a resolution (WD) of 2.1 nm. Local compensation of charge (by injecting nitrogen gas) or the sample shading was not necessary. Size distribution and 3D surface plot analysis were performed by application of Image J software to SEM microphotographs.

Transmission Electron Microscopy (TEM). Transmission electron microscopy was performed using a JEOL 100 CX II transmission electron microscope, operated at 100 kV with magnification of 100 000×. Observations were made in bright field. Powdered samples were placed on 2000 mesh cooper supports.

X-ray Powder Diffraction. Powder X-ray diffraction (XRD) data were collected with a Philips PW 1710 diffractometer with Cu Kα radiation (λ = 1.5418 nm) and graphite monochromator operated at 45 kV, 30 mA, and 25 °C.

FT-IR Spectroscopy. FT-IR experiments were done in a Nicolet FT-IR Nexus 470 spectrophotometer. To avoid coadsorbed water, the samples were dried under vacuum until constant weight was achieved and diluted with KBr powder before the FT-IR spectra were recorded.

Nitrogen Adsorption−Desorption Isotherms. The nitrogen isotherms at 73 K were measured with a Micrometrics model ASAPS (accelerated surface area and porosimetry system) 2020 instrument. Each sample was degassed at 373 K for 720 min at a pressure of 10^{-4} Pa.

UV−Vis and Fluorescence Spectroscopy. The UV−vis absorption and fluorescence spectra were recorded at 298 K by a UV−vis−NIR scanning spectrophotometer (Beckman, model DU 640) and a Varian Cary Eclipse spectrofluorometer (under excitation by UV light at 220 nm), respectively, using a 1 cm path length quartz cell. The spectrum was obtained for the anatase TiO_2 nanostructures that had been sonicated in ethanol to yield homogeneous dispersions. Pure ethanol solution was used as blank. Measurementes were performed at 298 K

Biomimetic Growth of Calcium Phosphate (CaP) Coating. To perform the bioactivity assay, the material was kept in contact with simulated body fluid (SBF) following the standard procedure described by Kokubo,[26] which has a composition and ionic concentration similar to that of human plasma, containing Na^+ (142.0 mM), K^+ (5.0 mM), Mg^{2+} (1.5 mM), Ca^{2+} (2.5 mM), Cl^- (148.8 mM), HCO^{3-} (4.2 mM), HPO_4^{2-} (1.0 mM), and SO_4^{2-} (0.5 mM). The prepared TiO_2 materials were soaked in SBF at 37 °C for periods of 1, 3, 6, and 10 days, then specimens were removed from fluid, rinsed with distilled water, and dried. The temperature was maintained by placing the samples in a thermostatted bath throughout the experiment.

RESULTS AND DISCUSSION

Reactive Microemulsion Precipitation. TiO_2 crystallites were generated from titanium(IV) tetrachloride ($TiCl_4$) by a

dx.doi.org/10.1021/la305080x | Langmuir 2013, 29, 2350−2358

reactive microemulsion precipitation process. The crystallographic structure of the synthesized crystals before and after annealing has been confirmed by X-ray diffraction, Figure 1a,b.

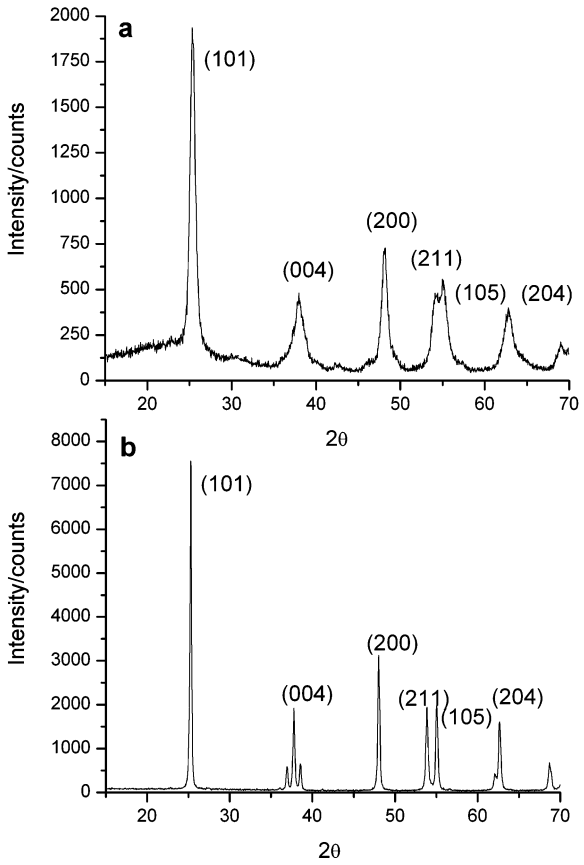

Figure 1. X-ray diffraction pattern of the synthesized anatase TiO_2 nanopowder (a) as prepared and (b) after hydrothermal treatment followed by calcination at 650 °C during 24 h in air flux.

The diffraction patterns in Figure 1 clearly indicate that the sample is a pure anatase phase (tetragonal, $I4_1/amd$, JCPDS card 21-1272). The absence of diffraction peaks at 27° and 31° shows that this sample was free from TiO_2 rutile and brookite structures. Furthermore, the nonexistence of a diffraction peak at 30° indicates the presence of long-range ordering in the TiO_2 nanoparticles.[32] The narrow reflection bands in the annealed material indicated that the nanopowders exhibit a high degree of crystallinity, Figure 1b. The anatase lattice parameters were computed from the XRD spectrum according to the following equations: $2d \sin\theta = \lambda$; $(1/d^2) = (h^2/a^2) + (k^2/b^2) + (l^2/c^2)$.[33] The obtained parameters are $a = b = 0.373$ nm and $c = 0.948$ nm, and these values agree with the literature report ($a = b = 0.3728$ nm and $c = 0.9502$ nm[33]).

The synthesis method is based on the use of microemulsions acting as chemical microreactors to control the particles' sizes and shapes. An emulsion is generally defined as a thermodynamically stable system composed of at least three components: two immiscible liquids (typically water and oil) and a surfactant.[34] The stability of the microemulsion, which affects the success of the synthesis, depends on several process parameters, in particular the water to oil ratio, the kind and content of emulsifier, the precursor concentration in the solution, and the mixing velocity. The prepared microemulsion system has an S_0 value 2 and 35 times higher than the W_0 and the Ti^{4+}/surfactant ratio, respectively. In addition, water/Ti^{4+} and oil/Ti^{4+} ratios are 20 times larger than the Ti^{4+}/surfactant ratio. Under these experimental conditions, there is a slow diffusion of Ti^{4+} ions through continuous organic phase in the aqueous microemulsion droplets. This situation prevents the $TiCl_4$ rapid hydrolysis and favors crystal morphology control. Scheme 1a shows the region that is chemically adequate for a precipitation reaction to take place and to form TiO_2 crystallites in the water pool, such as a microemulsion interface region. Fourier-transform infrared (FT-IR) spectroscopic studies have indicated that the water interior of a microemulsion droplet has a multilayered structure, consisting of interfacial, intermediate, and core water.[35] In our case, the interfacial layer is composed of water molecules directly bounded by polar head groups of AOT. Here the AOT hydrolysis released OH^- and RSO_3^- ions to react with Ti^{4+}.

According to the ligand field theory,[36] the crystallization of anatase and rutile TiO_2 should be via dehydration reaction among partially hydrolyzed $(Ti(OH)_xCl_y)^{2-}$ complexes, where $x + y = 6$.

Several ligands that contain $-COO^-$, $-CO$, and $-SO_3^-$ groups are stronger field ligands than Cl^- and OH^- ions and substitute them in the $(Ti(OH)_xCl_y)^{2-}$ complexes.[37,38] The AOT anion (RSO_3^-) possesses three oxygen atoms available for coordination with the metal atom. Sulfite (SO_3^-) ion presents the intriguing possibility that, in contrast to its dianionic relative CO_3^{2-}, all four of its atoms can in principle provide coordinate bonds to metal (M) centers.[39] The structures of a number of 1D, 2D, and 3D μ-sulfito–metal coordination polymers have been reported. Among these are electrically neutral chains and networks, some containing only metal and sulfite as in the "binary" metal sulfites $M_a(SO_3)_b$, whereas in others, neutral coligands such as H_2O, NH_3, and N-heterocycles are also bonded to the metal; there are also a few examples of anionic$[M_x(SO_3)_y]^{z-}$ arrangements. As an example, Abrahams et al.[39] described a very simple generation of the $Cu^I(SO_3)_4^{7-}$ ion, in which the metal center is in a tetrahedral environment of four sulfur donors, and demonstrate that it provides a versatile building block for the construction of mixed metal 1D, 2D and 3D coordination structures. So, it can be supposed that the reaction of RSO_3^- anions substitute the Cl^- anions in the hydrolysis process to form $(Ti(OH)_x(RSO_3)_z(Cl)_{y-z})^{n-}$ complexes and related species, Scheme 1b, with a higher stability than the $(Ti(OH)_x(Cl)_y)^{2-}$ complexes. The coordination of RSO_3^- anions leads to the inhibition of some crystal facets growth and the formation of small-sized anatase nanocrsytallites embryos with a characteristic shape (or facets exposed to surface). The concentrated HCl generated inside the microemulsion droplet pool during hydrothermal treatment not only should catalyze the nucleation of anatase but also the crystal growth via condensation of $(Ti(OH)_x(RSO_3)_z(Cl)_{y-z})^{n-}$ complexes.

Yan et. al[40] prepared nanocrystalline TiO_2 with different anatase/rutile ratios at low temperature by the microemulsion-mediated hydrothermal method. The effect of anions Cl^- and SO_4^{2-} on the contents of anatase and rutile phases in the TiO_2 powders have been successfully controlled by simply changing the proportion of Cl^- and SO_4^{2-} in the aqueous phase of the microemulsion. The content of the anatase phase increases with increasing concentration of SO_4^{2-} in the aqueous phase of the microemulsion in some range, and a large amount of SO_4^{2-} will only result in the presence of the anatase phase. It was found that bidentately bonding SO_4^{2-} species on TiO_6^{2-} octahedra is

dx.doi.org/10.1021/la305080x | Langmuir 2013, 29, 2350–2358

Scheme 1. (a) Microemulsion Precipitation Reaction Regions and (b) Reaction of RSO_3^- Anions Substituting the Cl^- Anions To Form $(Ti(OH)_x(RSO_3)_y(Cl)_z)^{n-}$ Complexes and Related Species

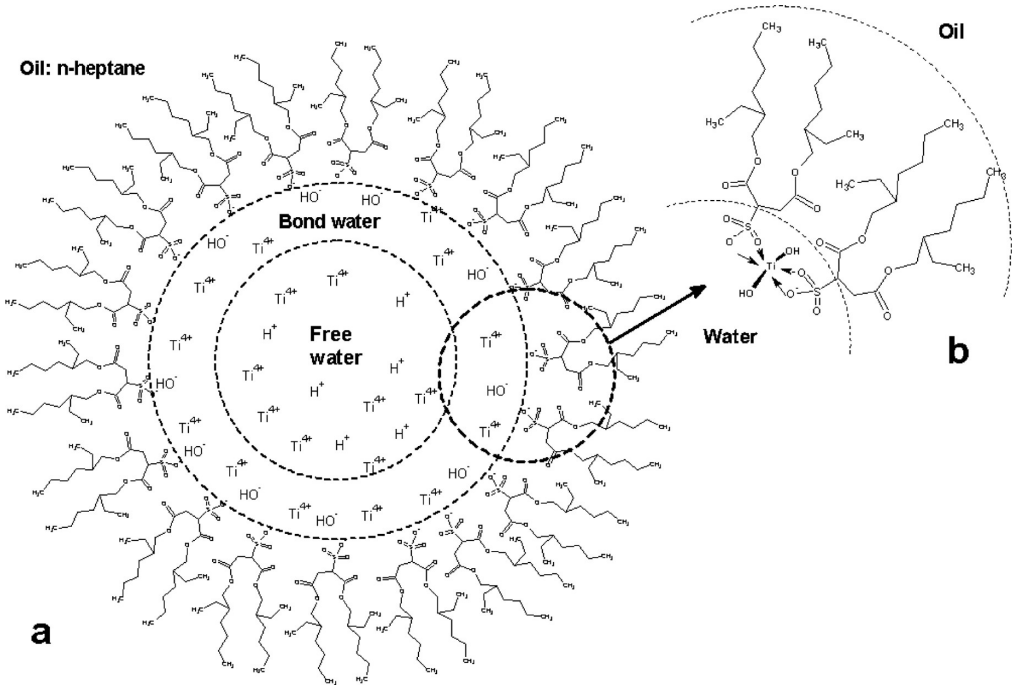

the main factor that affects the crystallite phase formation of TiO_2 during the preparation process.

Annealing at 640 °C increases the crystallinity of anatase powder, Figure 1. No phase transition from anatase to rutile (600 °C, at 1 atm[41]) was observed because the restrictive presence of AOT. This implies that the prepared TiO_2 cuboids are considerably thermostable.

Structural Studies. Scanning electron microscopy was used to characterize the surface morphology and sizes of the particles. Having been synthesized in emulsion droplets, the anatase TiO_2 powder mostly had a spherical morphology, Figure 2a. It was observed that the titania spheres were almost exclusively composed of mainly decahedral particles, i.e., truncated bipyramidal nanocrystallites, ranging in size (50−140 nm height and 60−150 nm width) but with the majority of 90 nm height and 89 nm width, Figure 3a. In addition, the 3D surface plot of nanocrystals surfaces (Figure 3b) indicated the existence of a uniform and dense surface morphology. From the symmetries of the well-faceted crystal structure, Figure 2b, the two flat squares are identified as {001} facets while the other eight isosceles trapezoidal surfaces are {101} facets which can be also revealed from the interfacial angle of 68.3°. The averaged aspect ratio (B/A),[42] which is defined by the ratio of short (B) and long (A) sides, was about 0.66−0.78. On the basis of SEM and TEM images, the percentage of highly reactive {001} facets is estimated to be approximately 45%. Again these values are similar than that of the decahedral particles prepared by Lu and co-workers, B/A = 0.80 corresponding to nearly 40% exposure of {001} facets to the total exposed facets.[10,11]

The BET specific surface area was found to be 11.91 $m^2\ g^{-1}$ by nitrogen adsorption measurements, much less than commercial anatase (Sigma Aldrich TiO_2, 99,7% anatase, CAS 1317-70-0, particle size <25 nm, and specific surface 200−220 $m^2\ g^{-1}$). In contrast to the case of regular anatase TiO_2 crystals which are usually dominated by the thermody-

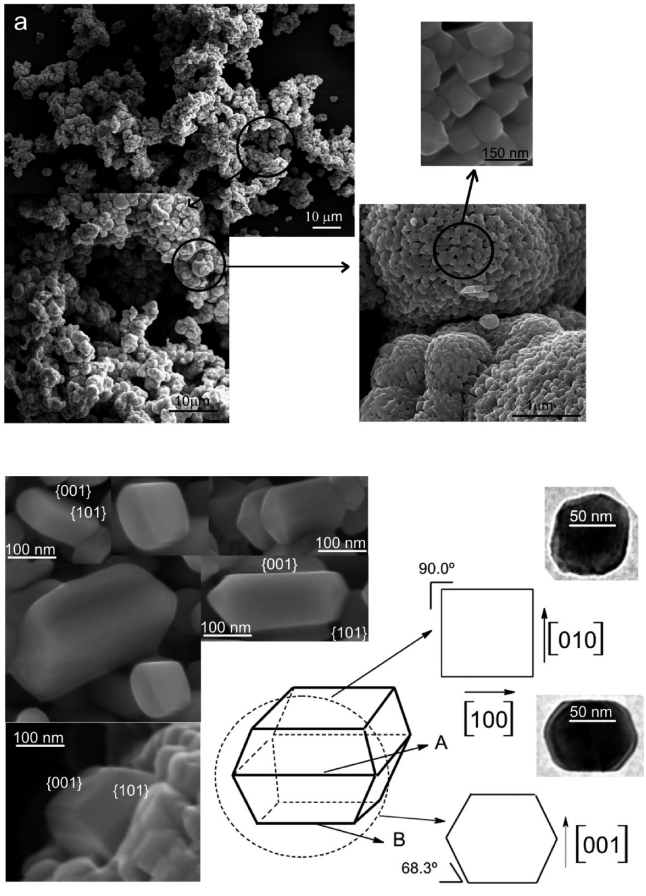

Figure 2. FE-SEM and TEM microphotographs of anatase TiO_2 samples: (a) the surface morphology and (b) truncated bipyramid nanocrystallites. SEM acquisition parameters: EHT = 3.00 kV, WD = 2.1 nm, signal A = in lens.

dx.doi.org/10.1021/la305080x | *Langmuir* 2013, 29, 2350−2358

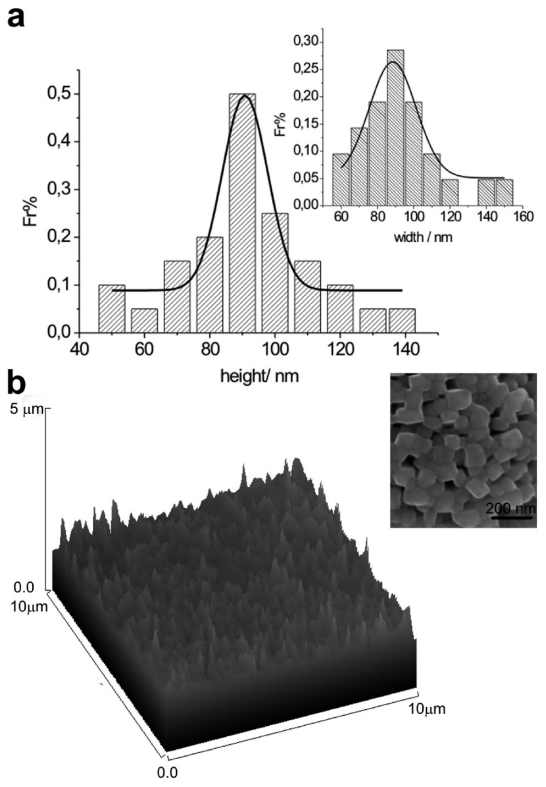

Figure 3. (a) Anatase TiO_2 nanocrystallites size distribution and (b) surface morphology.

namically stable {101} facets,[13] both {101} and {001} facets are clearly observed in microcrystallites. The appearance of highly reactive {001} facets, which are thermodynamically unstable due to the higher surface energy, is probably due to the most selective adsorption of organic units of AOT on the facets whose normal direction is [101], and this leads to the suppression of growth this way.

Photoluminescence Spectroscopy and Band Gap Energy. The photoluminescence (PL) emission spectrum of anatase TiO_2 sample measured at 298 K is shown in Figure 4.

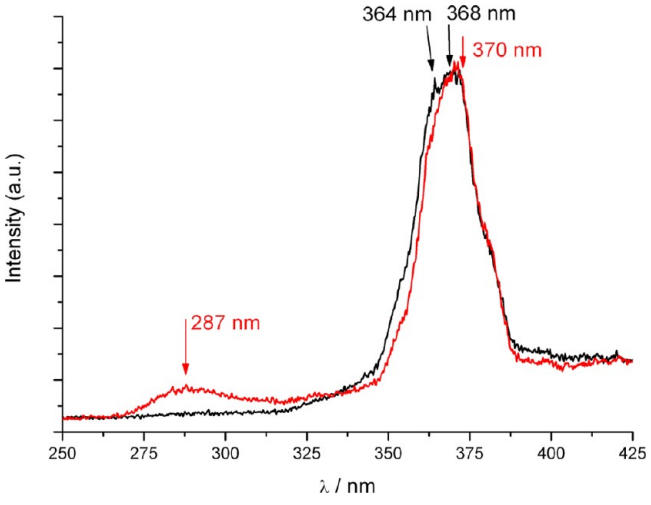

Figure 4. Photoluminescence (PL) emission spectrum of anatase cuboids with reactive {001} facets (black line) and commercial anatase TiO_2 (titanium(IV) dioxide 325 mesh, ≥99% anatase, Aldrich) sample dominated by the less-reactive {101} surfaces (red line).

At room temperature, a very weak PL spectrum was observed due to the rapid recombination rate of photoexcited electron/hole pairs. Commercial anatase shows two bands peaked at 287 nm and at 270 nm. On the basis of findings of Liu et al.,[43] the peak at 287 nm can be attributed to a direct vertical transition of photoinduced electrons and holes in TiO_2; it is very weak and disappears when the excitation light energy is lower than 3.87 eV (λ = 320 nm). The peak at 270 nm can be assigned to the band-to-band recombination because it is near-band-edge luminescence[44] and/or to the exciton trapped at shallow-level defects.[45] According to Liu et al.'s results[43] the self-exciton peaks are inevitable to widen and disappear due to strong phonon scattering at room temperature, so the band-to-band recombination is the more reasonable physical cause. Anatase dominated by the high-reactive {001} surfaces are characterized by two peaks centered at 364 and 368 nm, corresponding to the direct and indirect band gap transitions of TiO_2, respectively.[46] Evaluating the photoluminescence of single-crystalline anatase TiO_2 nanofibers with highly reactive (001) facets, Li et al.[46] yielded results similar to ours. However, Mercado et al.[47] indicated that, despite the preponderance of {001} surfaces in the TiO_2 nanosheet, samples exhibit a photoluminescence pattern that peaked at about 530 and 620 nm similar to that of conventional nanoparticles. They also evaluated photoluminescence defects from TiO_2 nanotubes with (110) and (100) facets exposed. Nanotubes exhibit a photoluminescence peak centered at ~580 nm that is blue-shifted and much weaker in comparison with the TiO_2 nanoparticles. They assigned the broad visible photoluminescence of anatase nanoparticles to two overlapping distributions: hole trap emission associated with oxygen vacancies on (101) exposed surfaces, which peaks in the green, and a broader emission extending into the red which results from electron traps on undercoordinated titanium atoms, which are prevalent on (001) facets. Moreover, the 1 μm diameter nanocuboids reported by Yang et al.,[48] in turns, showed a single broad photoluminescence peak centered at 426 nm. In light of the obtained results, we can state that the material luminescence is associated to its nanostructure and size rather than the presence of reactive facets. Nanosheets,[47] nanotubes,[47] and nanocuboids[48] have two large planar dimensions (diameter, length) showing orange and green emissions. However, nanofibers[46] with only one large dimension (length) have blue-violet emissions, likewise our nanoparticles.

Figure 5a shows the absorption spectrum of anatase TiO_2 in good agreement with previous results reported in the literature.[49] The absorption was due to the electron transition from O^{2-} antibonding to the lowest empty orbital of Ti^{4+} that is the electron transition from the valence band to the conduction band (band−band transition).[50] The band gap energy was estimated by plotting $(\alpha h\nu)^m$ of the polycrystalline TiO_2 against the photon energy ($h\nu$), as shown in Figure 5b. Where α is the absorption coefficient, $h\nu$ is the photon energy, and E_g is the band gap energy. Because only direct allowed transitions are considered, m = 2. The adsorption (A) is converted to the absorption coefficient using the following relationship:[51] $\alpha = (2.303 \times 10^3/lc)A\rho$, where A is the adsorption of the sample, ρ is the density of anatase TiO_2 (3.98 g cm^{-3}), l is the cuvette length (1 cm), and c is the concentration of the TiO_2 nanocrystals (2×10^{-5} g cm^{-3}). The band gap energy (3.18 eV) was determined by extrapolating the adsorption coefficient (α) to zero. The obtained value is slightly inferior to the band gap energy of anatase TiO_2 dominated by the less-reactive

dx.doi.org/10.1021/la305080x | Langmuir 2013, 29, 2350−2358

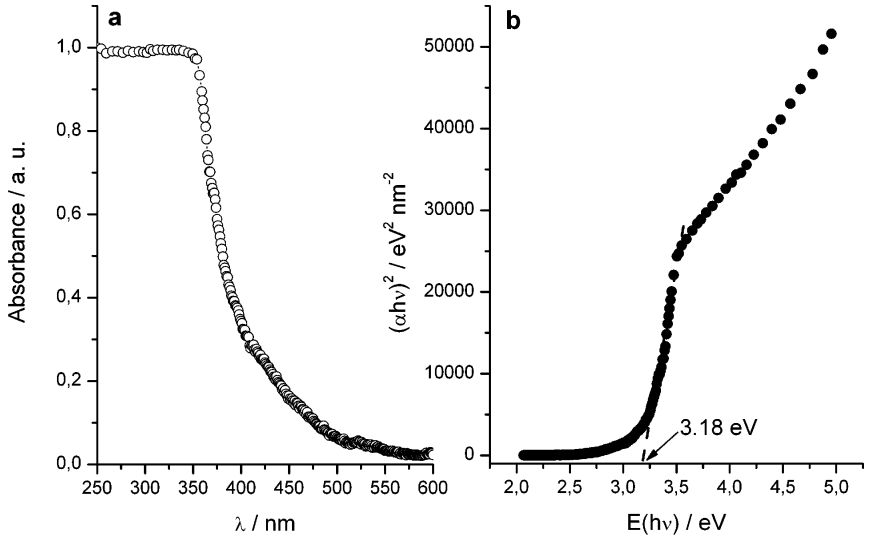

Figure 5. (a) Anatase TiO_2 absorption spectrum. (b) Estimation of band gap energy by plotting $(\alpha h\nu)^2$ vs $h\nu$.

{101} surface (3.20 eV[52]) and similar to those obtained by Liu et al.[49,53]

Biomimetic Growth of Calcium Phosphate (CaP) Coating. Biomimetic CaP deposition implies mimicking the natural process of mineralization, but without involving cellular and organic species. Biomimetic apatite deposition on sol−gel amorphous titanium oxide could not be detected,[54] and Li et al.[23] also reported that apatite is not biomimetically formed on single crystal of TiO_2 rhombohedral anatase. The formation of a negatively charged surface composed with Ti−OH is a key step of inducing growth of new CaP structures in a simulated body fluid, which for crystalline titanium dioxides can occur.[54,55] Certain types of Ti−OH groups in a specific structural arrangement are effective in inducing apatite nucleation. Nancollas et al.[55] explained that the surface tension of the metal oxides would influence the apatite epitaxial nucleation, and Uchida et al.[54] assumed that there are specific atomic arrangements in crystal structures suitable for the epitaxy of apatite growth. Moreover, Lindgren et al.[56] has investigated some boundary conditions for apatite formation on crystalline titanium oxide surfaces regarding the influence of coating thickness, soaking time, and soaking temperature. The soaking temperature had an effect on the HA formation and growth on both rutile surfaces and amorphous titanium oxide.

Therefore, it can be inferred that, besides the bulk material, interface properties are key factors producing the coating. Consequently, the growth of CaP coating is system and morphologically specific.

FT-IR spectra, Figure 6, indicate the changes at the surface composition of TiO_2 anatase samples after soaking in SBF at 37 °C for 1, 3, 6, and 10 days, respectively. Before treatment, only the adsorption characteristic band Ti−O−Ti appears in the 400−600 cm^{-1} region, which arises from the lattice vibration of TiO_2.[57] Surface modifications and the presence of calcium phosphate phases are noted from the first day of immersion. The broad adsorption bands around 3500 cm^{-1} and the bands between 1600 and 1650 cm^{-1} are due the incorporation of water molecules. The absorption band at 1428 and 1486 cm^{-1} come from carbonate υ_3 modes and are characteristics of a carbonate in an amorphous phase. The υ_2 mode of carbonate also gives sharp absorption at 874 cm^{-1}. Since this peak happens to overlap with the absorption from a P−O(H)

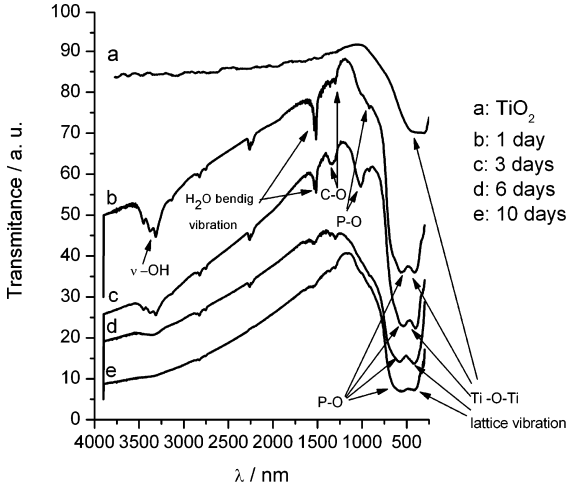

Figure 6. FT-IR of anatase TiO_2 surface composition after immersion in simulated body fluid (SBF).

stretching mode of possible HPO_4^{2-} ions,[58] the presence of HPO_4^{2-} ions cannot be excluded under experimental conditions. The strong and broad bands centered at 1056 and 566 cm^{-1} are assigned to the υ_3 P−O stretching and υ_4 bending modes of the phosphate, respectively. The 1056 cm^{-1} band appears featureless, also indicating the presence of an amorphous phase.[56] This agrees with the fact that no splitting in the 566 cm^{-1} band is observed which is another indication of amorphous calcium phosphate[59] presence. Beyond the 3 days of immersion of the material in SBF, infrared spectra show a broad band from 3500 to 2500 cm^{-1} masking the carbonate C−O and the P−O stretching vibration signals. The absorption band centered at 566 cm^{-1} becomes wider, probably due to the overlap with the band corresponding to the P−O(H) stretching mode band of HPO_4^{2-} ions. SEM microphotographs of anatase TiO_2 sample after soaking in SBF 3 days are shown in Figure 7. Elongated discs of about 1.3 μm length and 0.56 μm width can be appreciated on TiO_2 surface (not shown). These discs present the structure of a viscous gel and have a completely smooth surface that markedly differs from the rough surface of titania. From energy-dispersive X-ray spectroscopy (EDX) analysis, insets to Figure 7, it was confirmed that such structures

dx.doi.org/10.1021/la305080x | Langmuir 2013, 29, 2350−2358

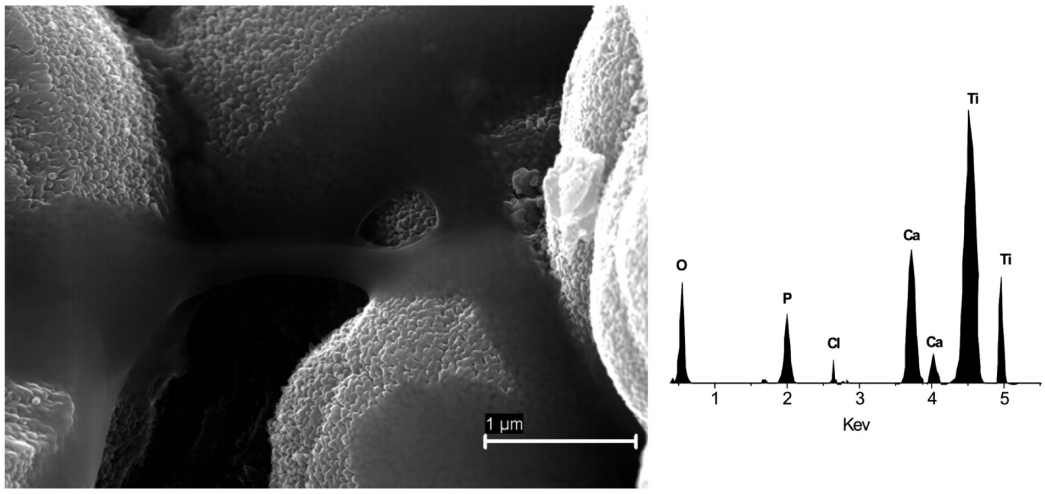

Figure 7. FE-SEM microphotographs of anatase TiO_2 samples after soaking in SBF for 3 days. Inset: EDX microanalysis of ATP clusters.

corresponded to compounds of Ca, P, and C with an atomic Ca/P ratio of about 1.5. Gel consistency is associated with a large amount of hydration water. These are typical characteristics of the amorphous tricalcium phosphate (ATCaP) phases, $Ca_3(PO_4)_2{\cdot}nH_2O$, and agrees with the analysis of FT-IR spectra. The morphology of ACP is still used as a distinctive feature to detect this phase in various systems.[28] The structure of ATCaP was first determined by Betts and Posner on the basis of the radial distribution function.[60] A short-range order was evident in ATCaP, corresponding to $Ca_9(PO_4)_6$ units with an average diameter of 0.95 nm, often referred as "Posner's clusters". The ATCaP contains a large amount of water; considered to be present in part in the intercluster space, allowing the association of Posner's clusters into large spherical units of 20−300 nm diameters (see Supporting Information). A second type of water, more loosely bound, would be simply adsorbed into these units transforming the disc-shaped associations into gel-like flocculates[28] as we can see from inspection of Figure 7.

CONCLUSION

In summary, we report a facile and controllable route for the synthesis of regular arranged decahedral anatase TiO_2 particles with high content of reactive {001} facets using a microemulsions droplet system at specific conditions as chemical microreactor. The emergence of highly reactive {001} facets, which are thermodynamically unstable due to its higher surface energy, is probably due to the selective adsorption of AOT anion (RSO^{3-}) organic units on the facets whose normal direction is [101] and to the suppression of the growth at this way. The obtained cuboids around 90 nm in size are thermostable and have a uniform and dense surface morphology with a BET specific surface area of 11.91 $m^2\ g^{-1}$ and a band gap energy (3.18 eV) slightly inferior to the anatase dominated by the less-reactive {101} facets (3.20 eV). Also, the particles show ultraviolet A (UVA) photoluminescence emissions at 364 and 368 nm. When compared to traditional methods, this procedure appears definitely cheaper and more easily applicable, as it does not require the use of hydrofluoric acid or high temperature conditions. Reactive facets on titania anatase favor the biomimetic growth of amorphous tricalcium phosphate after the first day of immersion in a simulated human plasma. Deposition of biomimetic ATCaP on titanium oxide surfaces, acting as a bonding layer, might improve boundlessly the integration of anchored implants and the biological responses to the host tissues, particularly in thinking of soft-tissue implants wherein ATCaP is usually biologically present.

ASSOCIATED CONTENT

Supporting Information

TEM microphotographs of cuboids anatase crystals, amorphous tricalcium phosphate (ATCaP) cluster size distribution, and anatase TiO_2 and ATCaP gel-like cluster surface morphology (SEM microphotographs). This material is available free of charge via the Internet at http://pubs.acs.org.

AUTHOR INFORMATION

Corresponding Author

*E-mail: pmessina@uns.edu.ar. Phone: +54 291 4595159. Fax: +54 291 4595160.

Notes

The authors declare no competing financial interest.

ACKNOWLEDGMENTS

The authors acknowledge Universidad Nacional del Sur (PGI 24/ZQ07), Concejo Nacional de Investigaciones Científicas y Técnicas de la República Argentina (CONICET, PIP-11220100100072), Xunta de Galicia (Project 10PXIB206258PR), and Education Audiovisual Culture, Executive Agency European Commission (EMUNDUS18) for their financial support. V.V. has a postdoctoral fellowship of CONICET. P.V.M. is an adjunct researcher of CONICET.

REFERENCES

(1) Fujishima, A.; Honda, K. Electrochemical photolysis of water at a semiconductor electrode. *Nature* **1972**, *238*, 37−38.

(2) Kominami, H.; Muratami, S.; Kato, J.; Kera, Y.; Ohtani, B. Correlation between some physical properties of titanium dioxide particles and their photocatalytic activity for some probe reactions in aqueous systems. *J. Phys. Chem B* **2002**, *106*, 10501.

(3) Schloegl, R. Energy: Fuel for thought. *Nat. Mater.* **2008**, *7*, 772−774.

(4) Sheppard, L. R.; Nowotny, J. Reactivity of TiO_2 with water and oxygen. Surface science perspective. *Adv. Appl. Ceram.* **2007**, *106*, 9−17.

(5) Yin, Y. B.; Zhao, X. P. Wormhole-like mesoporous Ce-oxide doped sol-gel nanosized titanium oxide. *Chem. Mater.* **2002**, *14*, 4633−4640.
(6) Peercy, P. S. The drive to miniaturization. *Nature* **2000**, *406*, 1023−1026.
(7) Borenstain, S. I.; Arad, U.; Lyubina, I.; Segal, A.; Warschawer, Y. Optimized random/ordered grating for an n-type quantum well infrared photodetector. *Appl. Phys. Lett.* **1999**, *75*, 2659−2661.
(8) Wang, R.; Hashimoto, K.; Fujishima, A. Light-induced amphiphilic surfaces. *Nature* **1997**, *338*, 431−432.
(9) Gong, X. Q.; Selloni, A. J. Reactivity of anatase TiO_2 nanoparticles: the role of the minority (001) surface. *J. Phys Chem. B* **2005**, *109*, 19560−19562.
(10) Yang, H. G.; Sun, C. H.; Qiao, S. Z.; Zou, J.; Liu, G.; Smith, S. C.; Cheng, H. M.; Lu, G. Q. Anatase TiO_2 single crystals with a large percentage of reactive facets. *Nat. Lett.* **2008**, *453*, 638−641.
(11) Yang, H. G.; Liu, G.; Qiao, S. Z.; Sun, C. H.; Jin, Y. G.; Smith, S. C.; Zou, J.; Cheng, H. M.; Lu, G. Q. Solvothermal synthesis and photoreactivity of anatase tio2 nanosheets with dominant {001} facets. *J. Am. Chem. Soc.* **2009**, *131*, 4078−4083.
(12) Wang, X.; Huang, B.; Wang, Z.; Qin, X.; Zhang, X.; Dai, Y.; Whangbo, M.-H. Synthesis of anatase TiO_2 tubular structures microcrystallites with a high percentage of {001} facets by a simple one-step hydrothermal template process. *Chem.—Eur. J.* **2010**, *16*, 7106 and references therein.
(13) Amano, F.; Prieto-Mahaney, O. O.; Terada, Y.; Yasumoto, T.; Shibayama, T.; Ohtani, B. Decahedral single-crystalline particles of anatase titanium (IV) oxide with high photocatalytic activity. *Chem. Mater.* **2009**, *21*, 2601−2606.
(14) Uchino, T.; Tokunaga, H.; Ando, M.; Utsumi, H. Quantitative determination of OH radical generation. *Toxicol. In Vitro* **2002**, *16*, 629−635.
(15) Xu, J.; Sun, Y.; Huang, J.; Chen, C.; Liu, G.; Jiang, Y.; Zhao, Y.; Jiang, Z. Photokilling cancer cells using highly cell-specific antibody−TiO_2 bioconjugates and electroporation. *Bioelectrochemistry* **2007**, *71*, 217−222.
(16) Seo, J. W.; Chung, H.; Kim, M. Y.; Lee, J.; Choi, I. H.; Cheon, J. Development of water-soluble single-crystalline TiO_2 nanoparticles for photocatalytic cancer-cell treatment. *Small* **2007**, *3*, 850−853.
(17) Rozhkova, E. A.; Ulason, I.; Lai, B.; Dimitrijevic, N. M.; Lesniak, M. S.; Rajh, T. A high-performance nanobio photocatalyst for targeted brain cancer therapy. *Nano Lett.* **2009**, *9*, 3337−3342.
(18) Wen, M.; Gu, J.-F.; Liu, G.; Wang, Z.-B.; Lu, J. Nanocrystalline titanium to mesoporous anatase with high bioactivity. *Cryst. Growth Des.* **2007**, *7*−*12*, 2400−2403.
(19) Salata, O. V. Applications of nanoparticles in biology and medicine. *J. Nanobiotechnol.* **2004**, *2*, 1−3.
(20) Mihranyan, A.; Forsgren, J.; Strømme, M.; Engqvist, H. Assessing surface area evolution during biomimetic growth of hydroxyapatite coatings. *Langmuir* **2009**, *25*, 1292−1295 and references therein.
(21) Gu, Y. W.; Tay, B. Y.; Lim, C. S.; Yong, M. S. Nanocrystallite apatite formation and its growth kinetics on chemically treated porous NiTi. *Nanotechnology* **2006**, *17*, 2212−2218.
(22) Kasuga, T.; Kondo, H.; Nogami, M. Apatite formation on TiO_2 in simulated body fluid. *J. Cryst. Growth* **2002**, *235*, 235−240.
(23) Li, P.; Ohtsuki, C.; Kokubo, T.; Nakanishi, K.; Soga, N.; de Groot, K. The role of hydrated silica inducing apatite on implants. *J. Biomed. Mater. Res.* **1994**, *28*, 7.
(24) Yang, Y.; Kim, K.-H.; Ong, J. L. A review on calcium-phosphate coatings produced using a sputtering process-an alternative to plasma spraying. *Biomaterials* **2005**, *26*, 327−337.
(25) Nguyen, H. Q.; Deporter, D. A.; Pilliar, R. M.; Valiquette, N.; Yakubovich, R. The effect of sol−gel-formed calcium phosphate coatings on bone ingrowth and osteoconductivity of porous-surfaced Ti alloy implants. *Biomaterials* **2004**, *25*, 865−876.
(26) Kokubo, T.; Kushitani, H.; Sakka, S.; Kisugi, T.; Yamamuro, T. Solutions able to reproduce in vivo surface-structure changes in bioactive glass−ceramic A-W3. *J. Biomed. Mater. Res.* **1990**, *24*, 721−734.
(27) Li, P.; Ohtsuki, C.; Kokubo, T.; Nakanishi, K.; Soga, N.; de Groot, K. A role of hydrated silica, titania, and alumina in forming biologically active bone-like apatite on an implant. *J. Biomed. Mater. Res* **1994**, *28*, 7−15.
(28) Combes, C.; Rey, C. Amorphous calcium phosphates: Synthesis, properties and uses in biomaterials. *Acta Biomater.* **2010**, *6*, 3362−3378 and references therein.
(29) Xia, W.; Lindahl, C.; Lausmaa, J.; Enqvist, H. Biomimetic hydroxyapatite deposition on titanium oxide surfaces for biomedical aplications. In *Advances in Biomimetics*; Cavrak M., Eds.; InTech: New York, 2011; Chapter 20, pp 429−452.
(30) Alexandridis, P.; Holzwarth, J. F.; Hatton, T. A. Interfacial dynamics of water-in-oil microemulsion droplets: Determination of the bending modulus using iodine laser temperature jump. *Langmuir* **1993**, *9*, 2045−2052.
(31) Alexandridis, P.; Holzwarth, J. F.; Hatton, T. A. Thermodynamics of droplet clustering in percolating AOT water-in-oil microemulsions. *J. Phys. Chem. B* **1995**, *99*, 8222−8232 and references therein.
(32) Trung, T.; Ha, C.-S. One-component solution system to prepare nanometric anatase TiO_2. *Mater. Sci. Eng.* **2004**, *C24*, 19−22.
(33) Chen, Y.; He, X.; Zhao, X.; Yuan, Q.; Gu, X. Preparation, characterization, and growth mechanism of a novel aligned nanosquare anatase in large quantities in the presence of TMAOH. *J. Colloid Interface Sci.* **2007**, *310*, 171 and references therein.
(34) Deorsola, F. A.; Vallauri, D. Study of the process parameters in the synthesis of TiO_2 nanospheres through reactive microemulsion precipitation. *Powder Technol.* **2009**, *190*, 304−309 and references therein.
(35) Wang, Y.; Zhou, A.; Yang, Z. Preparation of hollow TiO_2 microspheres by the reverse microemulsions. *Mater. Lett.* **2008**, *62*, 1930−1932 and references therein.
(36) Cheng, H.; Ma, J.; Zhao, Z.; Qi, L. Hydrothermal preparation of uniform nanosize rutile and anatase particles. *Chem. Mater.* **1995**, *7*, 663−671.
(37) Pärssinen, A.; Elo, P.; Klinga, M.; Leskelä, M.; Repo, T. Synthesis of novel titanium complexes bearing two mono anionic malonic acid ester based ligands and their use as catalyst precursors in ethene polymerisation. *Inorg. Chem. Commun.* **2006**, *9* (8), 859−861.
(38) Yin, H.; Wada, Y.; Kitamura, T.; Sumida, T.; Hasegawa, Y.; Yanagida, S. Novel synthesis of phase-pure nano-particulate anatase and rutile TiO_2 using $TiCl_4$ aqueous solutions. *J. Mater. Chem.* **2002**, *12*, 378−383.
(39) Abrahams, B. F.; Haywood, M. G.; Robson, R. $Cu(SO_3)_4^{7-}$: A readily accessible building block for new coordination polymers. *Cryst. Growth Des.* **2008**, *8* (4), 1288−1293.
(40) Yan, M.; Chen, F.; Zhang, J.; Anpo, M. Preparation of controllable crystalline titania and study on the photocatalytic properties. *J. Phys. Chem. B* **2005**, *109*, 8673−8678.
(41) Dachile, F.; Simons, P. Y.; Roy, R. Pressure-temperature studies of anatase, brookite, rutile and TiO_2-II. *Am. Mineral.* **1968**, *53*, 1929−1939.
(42) Barnard, A. S.; Curtiss, L. A. Prediction of TiO_2 nanoparticle phase and shape transitions controlled by surface chemistry. *Nano Lett.* **2005**, *5*, 1261−1266.
(43) Liu, B.; Wen, L.; Zhao, X. The photoluminescence spectroscopic study of anatase TiO_2 prepared by magnetron sputtering. *Mater. Chem. Phys.* **2007**, *106*, 350−353.
(44) Pan, D.; Zhao, N.; Wang, Q.; Jiang, S.; Ji, X.; An, L. Facile synthesis and characterization of luminescent TiO_2 nanocrystals. *Adv. Mater.* **2005**, *17*, 1991−1995.
(45) Suisalu, A.; Aarik, J.; Mändar, H.; Sildos, I. Spectroscopic study of nanocrystalline TiO_2 thin films grown by atomic layer deposition. *Thin Solid Films* **1998**, *336*, 295−298.
(46) Li, W.; Bai, Y.; Liu, W.; Liu, C.; Yang, Z.; Feng, X.; Lu, X.; Chan, K.-Y. Single-crystalline and reactive facets exposed anatase TiO2

nanofibers with enhanced photocatalytic properties. *J. Mater. Chem.* **2011**, *21*, 6718−6724.
(47) Mercado, C. C.; Knorr, F. J.; McHale, J. L.; Usmani, S. M.; Ichimura, A. S.; Saraf, L. V. Location of hole and electron traps on nanocrystalline anatase TiO_2. *J. Phys. Chem. C* **2012**, *116* (19), 10796−10804.
(48) Fang, W. Q.; Gong, X.-Q.; Yang, H. G. On the unusual properties of anatase TiO_2 exposed by highly reactive facets. *J. Phys. Chem. Lett.* **2011**, *2* (7), 725−734.
(49) Liu, G.; Sun, C.; Yang, H. G.; Smith, S. C.; Wang, L.; Lu, G. Q.; Cheng, H.-M. Nanosized anatase TiO_2 single crystals for enhanced photocatalytic activity. *Chem. Commun.* **2010**, *46*, 755−757.
(50) Mao, Y.; Wong, S. S. Size- and shape-dependent transformation of nanosized titanate into analogous anatase titania nanostructures. *J. Am. Chem. Soc.* **2006**, *128*, 8217−8226.
(51) Serpone, N.; Lawless, D.; Khairutdinov, R. Size effects on the photophysical properties of colloidal anatase TiO_2 particles: Size quantization versus direct transitions in this indirect semiconductor? *J. Phys. Chem.* **1995**, *99*, 16646−16654.
(52) Gärtner, M.; Dremov, V.; Müller, P.; Kisch, H. Bandgap widening of titania through semiconductor support interactions. *ChemPhysChem* **2005**, *6*, 714−718 and references therein.
(53) Liu, G.; Yu, J. C.; Lu, G. Q.; Cheng, H.-M. Crystal facet engineering of semiconductor photocatalysts: motivations, advances and unique properties. *Chem. Commun.* **2011**, *47*, 6763−6783.
(54) Uchida, M.; Kim, H. M.; Kokubo, T.; Fujibayashi, S.; Nakamura, T. Structural dependence of apatite formation on titania gels in a simulated body fluid. *J. Biomed. Mater. Res., Part A* **2003**, *64* (1), 164−170.
(55) Nancollas, G.; Wu, W.; Tang, R. The mechanism of crystallization and dissolution of calcium phosphates at surfaces. *Glastech. Ber. Glass. Sci.* **2000**, *73* (C1), 318−325.
(56) Lindgren, M.; Astrand, M.; Wiklund, U.; Enqvist, H. Investigation of boundary conditions for biomimetic HA deposition on titanium oxide surfaces. *J. Mater Sci. Mater. Med.* **2009**, *20* (7), 1401−1408.
(57) *The Infrared Spectra of Minerals*; Farmer, V. C., Ed.; Mineral Society: London, 1974.
(58) Apfelbaum, F.; Diab, H.; Mayer, I.; Faetherstone, J. D. B. An FTIR study of carbonate in synthetic apatites. *J. Inorg. Biochem.* **1992**, *45*, 277−282.
(59) Xu, G.; Aksay, I. A.; Groves, J. T. Continuous crystalline carbonate apatite thin films. A biomimetic approach. *J. Am. Chem. Soc.* **2001**, *123*, 2196−2203 and references therein.
(60) Betts, F.; Posner, A. F. A structural model of amorphous calcium phosphate. *Trans. Am. Crystallogr. Assoc.* **1974**, *10*, 73. Betts, F.; Posner, A. F. An X-ray radial distribution study of amorphous calcium phosphate. *Mater. Res. Bull.* **1974**, *9*, 353−360.